Journal of Biomedical Optics

SPIEDigitalLibrary.org/jbo

Retrospective respiration-gated whole-body photoacoustic computed tomography of mice

Jun Xia
Wanyi Chen
Konstantin Maslov
Mark A. Anastasio
Lihong V. Wang

SPIE

Retrospective respiration-gated whole-body photoacoustic computed tomography of mice

Jun Xia, Wanyi Chen, Konstantin Maslov, Mark A. Anastasio, and Lihong V. Wang*
Washington University in St. Louis, Optical Imaging Lab, Department of Biomedical Engineering, One Brookings Drive, Saint Louis, Missouri 63130

Abstract. Photoacoustic tomography (PAT) is an emerging technique that has a great potential for preclinical whole-body imaging. To date, most whole-body PAT systems require multiple laser shots to generate one cross-sectional image, yielding a frame rate of <1 Hz. Because a mouse breathes at up to 3 Hz, without proper gating mechanisms, acquired images are susceptible to motion artifacts. Here, we introduce, for the first time to our knowledge, retrospective respiratory gating for whole-body photoacoustic computed tomography. This new method involves simultaneous capturing of the animal's respiratory waveform during photoacoustic data acquisition. The recorded photoacoustic signals are sorted and clustered according to the respiratory phase, and an image of the animal at each respiratory phase is reconstructed subsequently from the corresponding cluster. The new method was tested in a ring-shaped confocal photoacoustic computed tomography system with a hardware-limited frame rate of 0.625 Hz. After respiratory gating, we observed sharper vascular and anatomical images at different positions of the animal body. The entire breathing cycle can also be visualized at 20 frames/cycle. [DOI: 10.1117/1.JBO.19.1.016003]

Keywords: photoacoustic computed tomography; small-animal whole-body imaging; respiratory motion; retrospective motion gating.

Paper 130724R received Oct. 6, 2013; revised manuscript received Nov. 20, 2013; accepted for publication Nov. 27, 2013; published online Jan. 6, 2014.

Photoacoustic tomography (PAT) is an emerging small-animal whole-body imaging technique that has drawn great interest in recent years.[1–6] PAT is based on the photoacoustic effect, which converts absorbed optical energy into pressure via thermoelastic expansion. The generated pressure waves are detected by ultrasonic transducers placed in multiple positions, and the complete dataset is then computed to reconstruct an image of the absorbed optical energy density in the tissue. The conversion to acoustic waves enables PAT to generate high-resolution images in the optically diffusive regime. In order to capture photoacoustic waves traveling along different directions, small-animal whole-body PAT systems typically have a large receiving aperture, achieved either by mechanically scanning a transducer array[4] or by using an array with a large number of elements.[1,7] However, even in the latter case, due to the limited number of data acquisition channels, it is challenging to capture signals from all elements with a single-laser shot. Therefore, the majority of whole-body PAT systems have a frame rate of <1 Hz. Due to acoustic distortion from the lungs, whole-body PAT systems mainly focus on regions below the chest, where respiration is the main cause of motion. Because a mouse breathes at up to 3 Hz, images acquired with a frame rate of <1 Hz are susceptible to respiratory motion artifacts. Respiratory gating is also essential in many imaging applications, where accurate localization of organs is required. For instance, in high-intensity focused ultrasound (HIFU) tumor treatment, the respiration-induced organ displacement can be larger than the focus of the treatment beam.[8]

To reduce respiratory motion, whole-body PAT imaging has employed different animal mounting schemes. For instance, Brecht et al.[4] used pretensioned fiberglass rods to minimize animal movement. Lam et al.[9] laid the animal on its back to image the kidney region. However, all these approaches can only partially resolve the problem, and they are only applicable to the specific system. In this report, we propose a retrospective respiratory gating method that is widely applicable to different whole-body PAT systems. In our approach, the respiratory waveform is recorded during photoacoustic data acquisition, where photoacoustic signals from different views are captured at a constant speed as usual. After the experiment, the entire dataset is sorted and clustered according to respiratory phases. We then reconstruct the photoacoustic image using only data acquired from the same respiratory phase, greatly diminishing respiratory motion artifacts.

A key requirement of this approach is the accurate monitoring of the animal's respiratory waveform. Because photoacoustic experiments require water coupling, the animal is fully or partially immersed in water. Therefore, conventional electrical-based respiratory monitoring approaches, such as impedance pneumography,[10] cannot be employed. In addition, to ensure transmission of both light and sound, we cannot mount any opaque devices, such as a pressure sensor or a strain gage, on the animal body. Alternatively, one can use intubation and ventilation to precisely control the breathing cycle.[11] However, that procedure requires special training, and repeated intubation for longitudinal monitoring may damage the animal's trachea or vocal cords.[12] Here, we devise an approach that takes advantage of the water coupling. In this approach, a pressure sensor is used to continuously monitor fluctuations in the water level, which directly correlates to changes in the animal's corporeal volume. This method demands minimal hardware modification and is applicable to any whole-body PAT system.

*Address all correspondence to: Lihong V. Wang, E-mail: lhwang@wustl.edu

0091-3286/2014/$25.00 © 2014 SPIE

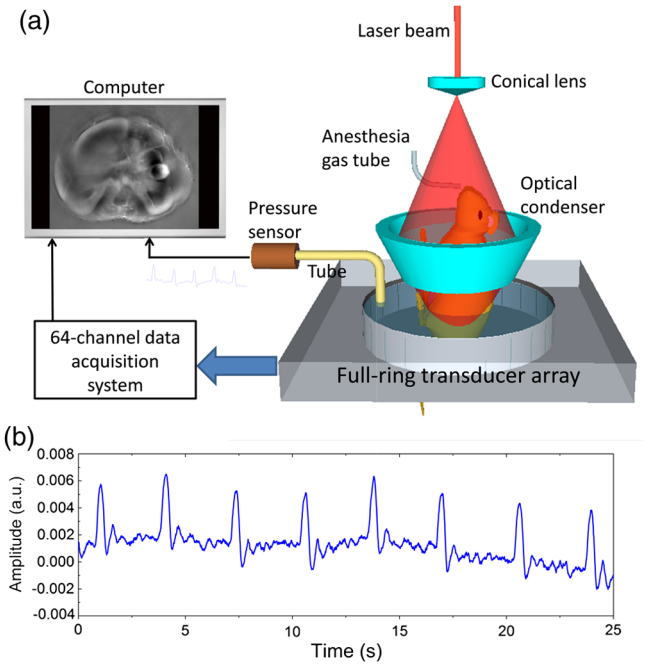

Fig. 1 (a) Schematic diagram of the ring-shaped confocal photoacoustic computed tomography system with respiratory motion gating. (b) A section of the respiratory waveform as monitored by the pressure sensor.

Figure 1(a) is a schematic diagram of the ring-shaped confocal photoacoustic computed tomography (RC-PACT) system with respiratory motion detection. A 10-Hz pulse-repetition rate Ti:sapphire laser (LS-2137, Symphotic TII) is used as the excitation source. The laser beam is first converted into a ring-shaped beam by a conical lens and then redirected to the animal body by an optical condenser. The photoacoustic signals are detected by a 512-element full-ring transducer array with 5-MHz central frequency and >80% bandwidth.[13] The array data is acquired by a 64-channel data acquisition system (DAQ) with 40-MHz sampling rate. Due to the limited data transfer speed, the DAQ system can capture data from only every other laser shot, yielding a full-ring acquisition time of 1.6 s. A detailed description of the imaging system and animal mounting schemes can be found in Refs. 1, 2, and 14. To capture the respiratory waveform, we used a pressure sensor (PXCPC, OMEGA Engineering Inc., Stamford, Connecticut). As shown in Fig. 1(a), the input of the pressure sensor is connected to a plastic tube. The other end of the tube is immersed in the coupling water, which compresses the air in the tube. Therefore, when the water level varies, the air pressure in the tube also changes. The output of the pressure sensor is amplified and then digitized by a data acquisition system (PCI-6220, National Instruments, Austin, Texas) at a 100-Hz sampling rate. Figure 1(b) shows a section of the pressure signal acquired over 25 s. Pressure peaks due to periodic breathing can be clearly seen for every 3 s.

The data processing steps are illustrated in Fig. 2. In each experiment, we continuously acquire 180 image frames over a span of 4.8 min and then sort the data according to the respiratory waveform. For signals acquired at each laser shot, we first identify the temporal position in the respiratory waveform and then assign it a phase value, ranging from 0% to 100%, determined by its relative position between two adjacent respiratory peaks. The data are then sorted according to the respiratory phase and evenly clustered into 20 sets. The number of clusters is chosen to ensure that each cluster contains data from all 512 transducer elements, i.e., a full 2π imaging aperture is covered. Due to 8:1 multiplexing, the full-ring array is divided into eight segments, and each laser pulse generates data from one segment. Within a cluster, different array segments may have produced data with different numbers of copies. Therefore, we first average the data from each segment according to its number of copies and then combine all of them to form a single full-ring dataset, which is used to reconstruct a photoacoustic image for the given cluster. Merging images from all clusters produces a continuous video of the entire respiratory cycle. Because photoacoustic image reconstruction is also a data averaging process, the effect of the different number of data copies at each array segment is mitigated after the reconstruction. As each cluster has approximately the same total number of data copies ($180 \times 8/20$), the final reconstructed image at each frame has a similar signal-to-noise ratio. To mitigate image artifacts induced by acoustic reflectors, such as the spine and GI tract, we used the half-time image reconstruction principle.[15] Because the main purpose of this study was to compensate for respiratory motion, rather than performing quantitative analysis, a noniterative half-time reconstruction algorithm was employed that is operated by directly back-projecting the first half of the raw data.

Figure 3 shows *in vivo* cross-sectional images acquired from the liver region of a 2-month-old nude mouse. The mouse was anesthetized with isoflurane, which slowed its respiratory rate to 1.25 s/breath. Without motion compensation, each image frame is thus acquired over a period of 1.28 (i.e., 1.6/1.25) breathing cycles with eight laser pulses. As expected, the ungated image [Fig. 3(a)] is appreciably more blurry than the gated image [Fig. 3(b)], especially for the hepatic vasculature. The skin boundary and cross sections of main blood vessels, such as vena cava, are also less clear in the ungated image due to the respiratory motion.

To better illustrate the respiratory effect, we plot the temporal changes of photoacoustic amplitude from a small region marked with red circles in Figs. 3(a) and 3(b). Both Figs. 3(c) and 3(d) contain data from 90 frames of images of the red circled region. It can be seen that respiratory gating not only allows us to visualize the breathing cycle coherently but also improves the temporal resolution. In Fig. 3(d), we can see the amplitude drop with body expansion, which moves the skin vessel out of the red circled region. In contrast, Fig. 3(c) shows only randomized amplitude fluctuation. Video 1 shows the ungated images acquired at 1.6 s/frame, and Video 2 shows the gated images resampled to 0.065 s/frame, corresponding to 20 frames/

Fig. 2 Flow chart illustrating the data processing steps.

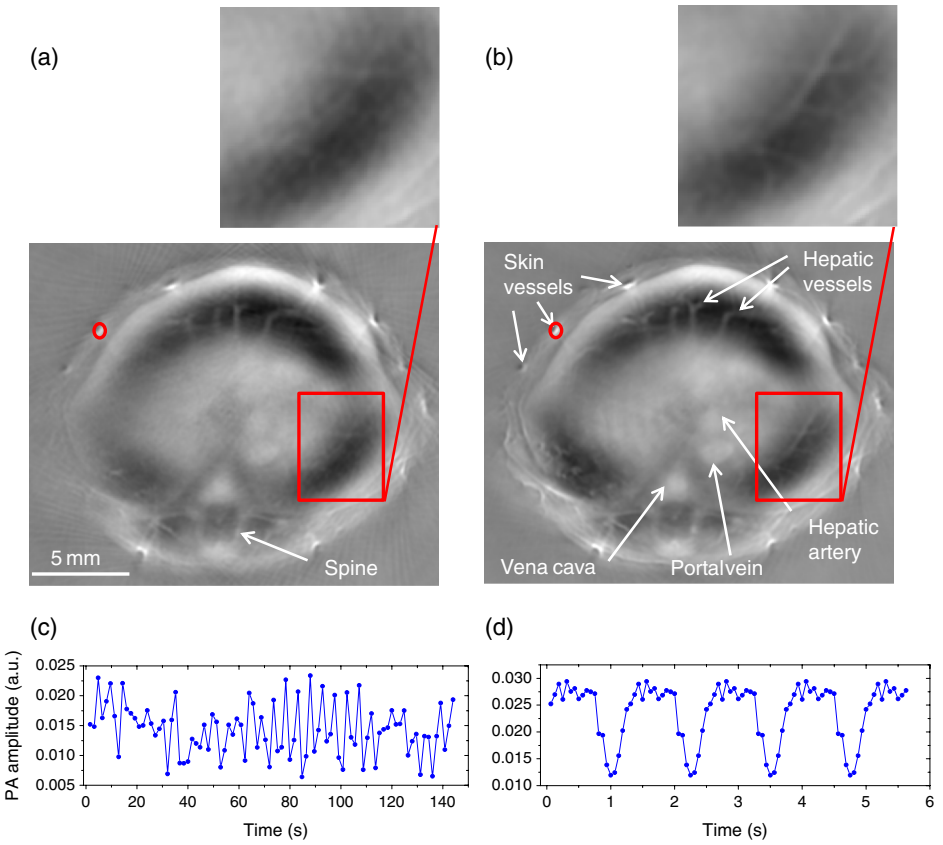

Fig. 3 *In vivo* mouse cross-sectional photoacoustic images acquired around the liver region. (a) Image reconstructed without respiratory motion gating (Video 1, MPEG, 2.47 MB) [URL: http://dx.doi.org/10.1117/1.JBO.19.1.016003.1]. (b) Image reconstructed with respiratory motion gating (Video 2, MPEG, 10.6 MB) [URL: http://dx.doi.org/10.1117/1.JBO.19.1.016003.2]. The hepatic vessels in the red box are enlarged to show the effect of respiratory motion correction. (c) and (d) show temporal changes in photoacoustic amplitude within the red circled regions in (a) and (b), respectively. Video 3, MPEG, 10.9 MB) [URL: http://dx.doi.org/10.1117/1.JBO.19.1.016003.3] was generated using a single copy of data at each respiratory phase. The motion-gated image and videos were reconstructed from data acquired over 4.8 min.

respiratory cycle. Compared to the random body movements seen in Video 1, we clearly see the rhythmic respiratory expansion and contraction of the animal body. It should be noted that the resampled 15.4-Hz (i.e., $1/0.065$ s) frame rate is faster than the 10-Hz laser pulse repetition rate. This improvement is due to both the noninteger ratio of the laser's pulse repetition rate (10 Hz) to the respiratory rate (~0.8 Hz) and the fluctuation of the respiratory cycle (±4% over the imaging period).

It should be emphasized that the role of respiratory gating is twofold. First, it improves the image sharpness because image reconstruction is performed using only data acquired at the same respiratory phase. Second, it improves the signal-to-noise ratio, as data acquired at the same respiratory phase can be constructively averaged. To better illustrate the two effects, we attached Video 3, which was generated using only a single copy of data at each respiratory phase (without constructive averaging). It can be seen that while the vessel sharpness here is comparable to that in Video 2, the ring-shaped electronic noise is more noticeable.

We also imaged the kidney region, where more organs can be visualized. Although the kidneys are farther away from the lungs than the liver, the effect of respiratory motion is still evident. The kidneys, spleen, spine, and vascular network in the uncorrected Fig. 4(a) are more blurred than the counterparts in the motion-compensated Fig. 4(b). The skin and abdominal vessels are also difficult to identify in Fig. 4(a). We also plot in Figs. 4(c) and 4(d) the temporal photoacoustic signal changes within a red circle placed in between the skin and spleen. In Fig. 4(d), we can clearly see the signal increase due to body expansion, which moves the spleen to the red circled region. The ungated and gated imaging frames are also compiled as Videos 4 and 5, respectively. The rhythmic respiratory motion of the animal body, as well as the movements of its organs, can be clearly observed in Video 5.

The rate of animal respiration can be slowed by increasing the isoflurane concentration in the inhalation gas. In another study, we imaged a mouse with a respiratory rate of ~0.31 Hz, which is slower than our imaging frame rate (0.625 Hz). Figures 5(a) and 5(b) compare the ungated and gated images. Although the blurs caused by the respiratory motion are not as obvious as in the previous cases, the hepatic vascular structures are still clearer in the motion-compensated image [Fig. 5(b)]. In addition, the signal-to-noise ratio is also improved, as can be seen from the disappearance of the system's electronic-noise artifact in Fig. 5(b). Because each gated image is an average of approximately nine (180/20) projections, the signal–to-noise ratio is improved by three times. Therefore, even when the respiratory rate is slower than the imaging frame rate, respiratory gating is still beneficial. Figures 5(c)

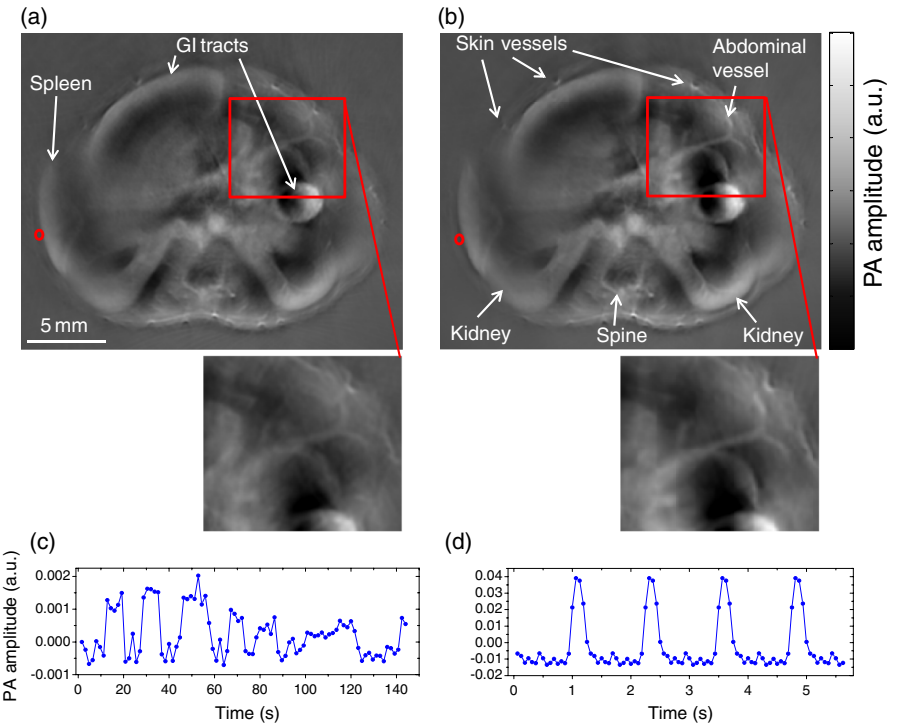

Fig. 4 *In vivo* small-animal cross-sectional photoacoustic images acquired around the kidney region. (a) Image reconstructed without respiratory motion gating (Video 4, MPEG, 2.75 MB) [URL: http://dx.doi.org/10.1117/1.JBO.19.1.016003.4]. (b) Image reconstructed with respiratory motion gating (Video 5, MPEG, 11.8 MB) [URL: http://dx.doi.org/10.1117/1.JBO.19.1.016003.5]. The abdominal vessels are enlarged to show the effect of respiratory motion correction. (c) and (d) show temporal changes in photoacoustic amplitude within the red circled regions in (a) and (b), respectively. The motion-gated image and video were reconstructed from data acquired over 4.8 min.

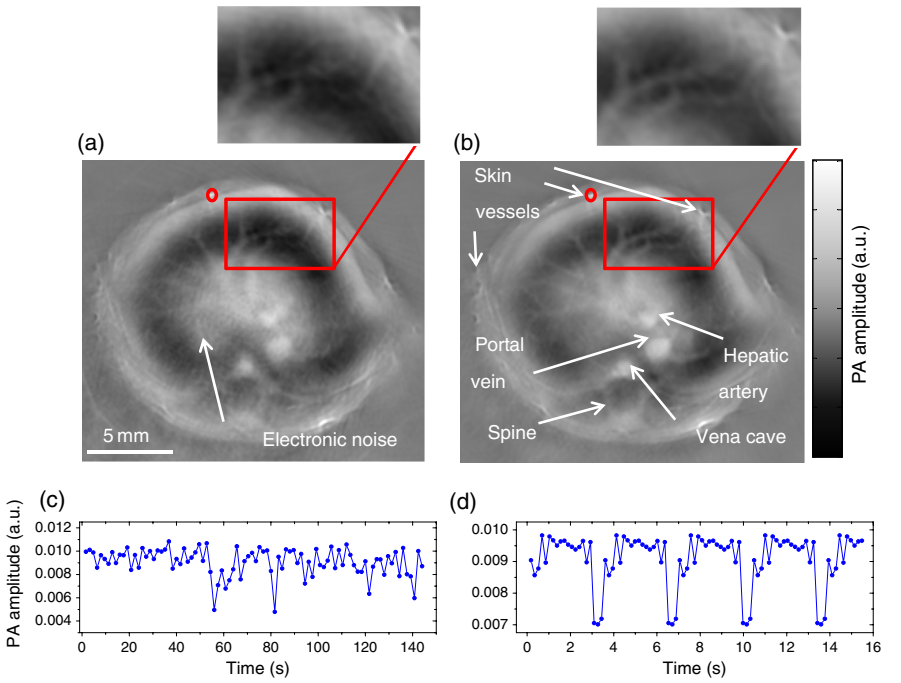

Fig. 5 *In vivo* small-animal cross-sectional photoacoustic images acquired around the liver region. (a) Image reconstructed without respiratory motion gating (Video 6, MPEG, 2.16 MB) [URL: http://dx.doi.org/10.1117/1.JBO.19.1.016003.6]. (b) Image reconstructed with respiratory motion gating. The hepatic vessels are enlarged to show the effect of respiratory motion (Video 7, MPEG, 9.22 MB) [URL: http://dx.doi.org/10.1117/1.JBO.19.1.016003.7]. (c) and (d) show temporal changes in photoacoustic signal within the red circled regions in (a) and (b), respectively. The motion-gated image and video were reconstructed from data acquired over 4.8 min.

and 5(d) show changes in photoacoustic amplitude within the red circles in Figs. 5(a) and 5(b), respectively. As expected, Fig. 5(d) shows periodic drop in photoacoustic amplitude due to body expansion, which moves the skin vessel out of the red circled region. Compared to Fig. 4(d), Fig. 5(d) has a longer resting period between breaths. This phenomenon is commonly observed in respiratory depression caused by high isoflurane concentrations.[16] The same effect can also be seen in Video 7.

In summary, we implemented, for the first time, respiratory gating in mouse whole-body PAT. Taking advantage of the water coupling, we used a pressure sensor to monitor the water level fluctuation induced by animal respiration. This noninvasive procedure lends itself to other whole-body PAT systems. We demonstrated the improvement in imaging quality under different respiratory rates and at multiple anatomical locations. Respiratory gating also allows us to sort and resample the data to a much higher frame rate, allowing visualization of the entire breathing cycle. In the respiration-gated videos (videos 2, 3, 5, and 7), we can clearly see the rhythmic movement of the liver, spleen, and kidneys. Because the respiratory waveform can be accessed in real time, after a control experiment is performed, our gating method can also potentially permit accurate tumor targeting during HIFU (Ref. 8) and radiation[17] therapies.

In the current study, because our excitation laser could not be triggered at a rate other than 10 Hz, we opted for retrospective respiratory gating. Using laser systems with flexible triggering options, we can also employ prospective respiratory gating, which can be used for high-speed imaging of a chosen respiratory phase. The same data processing principle can be used for cardiac gating. Compared to image-based gating approaches,[18] monitoring of the respiratory or cardiac waveform is immune to image noises and the data processing is computationally less intensive. Therefore, we expect that our proposed method will be widely used to improve the image quality and broaden the applications of small-animal whole-body PAT.

Acknowledgments

The authors appreciate Prof. James Ballard's close reading of the manuscript. This work was sponsored in part by National Institutes of Health grants DP1 EB016986 (NIH Director's Pioneer Award), R01 EB016963, R01 CA134539, R01 EB010049, and R01 CA159959. L.W. has a financial interest in Microphotoacoustics, Inc. and Endra, Inc., which, however, did not support this work. K.M. has a financial interest in Microphotoacoustics, Inc., which, however, did not support this work.

References

1. J. Xia et al., "Whole-body ring-shaped confocal photoacoustic computed tomography of small animals in vivo," *J. Biomed. Opt.* **17**(5), 050506 (2012).
2. M. R. Chatni et al., "Tumor glucose metabolism imaged in vivo in small animals with whole-body photoacoustic computed tomography," *J. Biomed. Opt.* **17**(7), 076012 (2012).
3. G. S. Filonov et al., "Deep-tissue photoacoustic tomography of a genetically encoded near-infrared fluorescent probe," *Angewandte Chemie Int. Edition* **51**(6), 1448–1451 (2012).
4. H.-P. Brecht et al., "Whole-body three-dimensional optoacoustic tomography system for small animals," *J. Biomed. Opt.* **14**(6), 064007 (2009).
5. L. V. Wang and S. Hu, "Photoacoustic tomography: in vivo imaging from organelles to organs," *Science* **335**(6075), 1458–1462 (2012).
6. J. Xia and L. Wang, "Small-animal whole-body photoacoustic tomography: a review," *IEEE Trans. Biomed. Eng.* **PP**(99), 1–10 (2013).
7. L. Xiang et al., "4-D photoacoustic tomography," *Sci. Rep.* **3**(1113), 1–8 (2013).
8. M. Pernot, M. Tanter, and M. Fink, "3-D real-time motion correction in high-intensity focused ultrasound therapy," *Ultrasound Med. Biol.* **30**(9), 1239–1249 (2004).
9. R. B. Lam et al., "Dynamic optical angiography of mouse anatomy using radial projections," *Proc. SPIE* **7564**, 756405 (2010).
10. V. P. Seppa, J. Viik, and J. Hyttinen, "Assessment of pulmonary flow using impedance pneumography," *IEEE Trans. Biomed. Eng.* **57**(9), 2277–2285 (2010).
11. D. Cavanaugh et al., "In vivo respiratory-gated micro-CT imaging in small-animal oncology models," *Mol. Imaging* **3**(1), 55–62 (2004).
12. A. Oshodi et al., "Airway injury resulting from repeated endotracheal intubation: possible prevention strategies," *Pediatr. Crit. Care Med.* **12**(1), E34–E39 (2011).
13. J. Gamelin et al., "A real-time photoacoustic tomography system for small animals," *Opt. Express* **17**(13), 10489–10498 (2009).
14. J. Xia et al., "Three-dimensional photoacoustic tomography based on the focal-line concept," *J. Biomed. Opt.* **16**(9), 090505 (2011).
15. M. A. Anastasio et al., "Half-time image reconstruction in thermoacoustic tomography," *IEEE Trans. Med. Imaging* **24**(2), 199–210 (2005).
16. D. R. Cleary et al., "A novel, non-invasive method of respiratory monitoring for use with stereotactic procedures," *J. Neurosci. Methods* **209**(2), 337–343 (2012).
17. M. H. Phillips et al., "Effects of respiratory motion on dose uniformity with a charged particle scanning method," *Phys. Med. Biol.* **37**(1), 223–234 (1992).
18. A. Taruttis et al., "Motion clustering for deblurring multispectral optoacoustic tomography images of the mouse heart," *J. Biomed. Opt.* **17**(1), 016009 (2012).

Jun Xia earned his PhD degree at the University of Toronto and is currently a postdoctoral fellow at Washington University in St. Louis, under the mentorship of Dr. Lihong V. Wang. His research interests are the development of novel biomedical imaging techniques including photoacoustic, photothermal and ultrasonic imaging. He has published more than 20 peer-reviewed journal articles in photoacoustic and photothermal research.

Wanyi Chen is currently an undergraduate student at Washington University in St. Louis and a research assistant in Dr. Lihong V. Wang's lab. Her research interests are in photoacoustic and ultrasonic imaging.

Konstantin Maslov graduated from Moscow Institute of Physics and Technology, Moscow, Russia and received a PhD in physical acoustics from Moscow State University, Russia, in 1993. Currently, he is a research associate professor in the Biomedical Engineering department at Washington University in St Louis, Missouri. His research interests include ultrasonics, optical, photoacoustic and photothermal imaging.

Mark A. Anastasio earned his PhD degree at the University of Chicago and is currently a professor of biomedical engineering at Washington University in St. Louis. His research interests include tomographic image reconstruction, imaging physics, and the development of novel computed biomedical imaging systems. He has conducted extensive research in the fields of diffraction tomography, x-ray phase-contrast x-ray imaging, and photoacoustic tomography.

Lihong V. Wang earned his PhD degree at Rice University, Houston, Texas. He currently holds the Gene K. Beare distinguished professorship of Biomedical Engineering at Washington University in St. Louis. He has published 342 peer-reviewed journal articles and delivered 370 keynote, plenary, or invited talks. His Google Scholar h-index and citations have reached 81 and over 26,000, respectively.